PAPER

Facets of reaction mechanism in $^{6}Li+^{181}Ta$ system

IOP Publishing Journal of Physics G: Nuclear and Particle Physics
J. Phys. G: Nucl. Part. Phys. **50** (2023) 025106 (22pp) https://doi.org/10.1088/1361-6471/acaffc

Facets of reaction mechanism in ^{6}Li+^{181}Ta system

Rishabh Kumar, Rinku Prajapat and Moumita Maiti*

Department of Physics, Indian Institute of Technology Roorkee, Roorkee 247667, Uttarakhand, India

E-mail: moumita.maiti@ph.iitr.ac.in

Received 18 October 2022, revised 18 December 2022
Accepted for publication 4 January 2023
Published 25 January 2023

Abstract

More focused investigations are required to better understand the different modes of fusion phenomena in weakly bound projectiles. In order to comprehend the reaction mechanism of weakly bound projectiles, a new measurement of the evaporation residue cross sections from the ^{6}Li-induced reaction on ^{181}Ta in the 4.5–7.1 MeV/nucleon energy range has been reported in this article. The γ-ray spectrometry has been employed to identify the ^{183m,g}Os, ^{182}Os, ^{183}Re, and ^{183,182m2,180}Ta residues produced in the reaction via different evaporation channels. The EMPIRE-3.2.2 code, which houses both the equilibrium and pre-equilibrium models in its framework, and PACE4 have been tasked to analyze the measured excitation functions. Out of the two, EMPIRE-3.2.2 demonstrates better agreement with the data. A systematic analysis of the measured data and theoretical background indicates that the complete and incomplete fusion of ^{6}Li contribute to the residual cross sections. Thus, the strength of the partial fusion has been inferred. Further, the neutron transfer channels have been found to contribute significantly to the reaction dynamics; hence they are investigated using the coupled reaction channel calculations and discussed in detail. The isomeric cross section ratio obtained from the measured residual cross sections of the isomeric pair of ^{183}Os highlights the significance of angular momentum and relative spins of the ground and isomeric states as a function of projectile incident energy.

Keywords: weakly bound projectile, incomplete fusion, neutron transfer, coupled-channel calculation, residual cross section measurement, ^{6}Li-induced reactions

(Some figures may appear in colour only in the online journal)

* Author to whom any correspondence should be addressed.

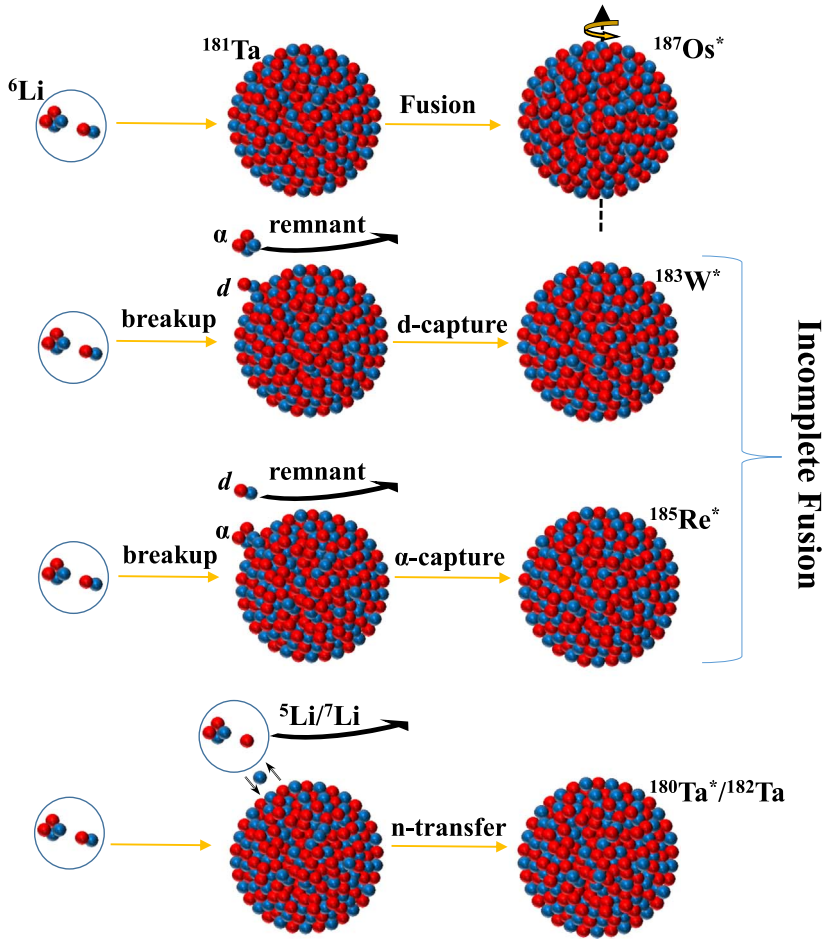

Figure 1. A schematic diagram showcasing different reaction processes ought to occur in the ^{6}Li+^{181}Ta reaction.

1. Introduction

Understanding fusion phenomena based on coupling effects to collective degrees of freedom has been a driving question in nuclear physics for over a few decades. Also, analysis of high-quality fusion data can harness useful information about nuclear interactions at distances corresponding to the outer side of the Coulomb barrier [1]. Moreover, the measurement of fusion cross sections deep into the barrier provides tools to extract astrophysical reaction rates. Several experimental and theoretical studies show that low-lying collective inelastic excitations may lead to large sub-barrier fusion enhancement compared to the predictions of one-dimensional barrier penetration models (1DBPM), specifically for highly deformed nuclei. Furthermore, transfer reactions are known to play a vital role in enhancing fusion cross sections in close vicinity of the Coulomb barrier. Since couplings to the bound states seem to underplay at energies far above the barrier, the fusion excitation function at such energies is generally well described by 1DBPM [2].

A particular case of fusion with weakly bound projectiles (WBPs) arises as it showcases a significant reduction of complete fusion (CF) cross sections compared to strongly bound projectiles at energies above the Coulomb barrier. Generally, the WBPs are nuclei having binding energy (BE) less than 3 MeV [3]. These WBPs can further be classified as stable (viz. ^{6,7}Li and ^{9}Be) and radioactive (^{6}He, ^{11}Li, etc); possessing a general $\alpha + x$ cluster structure. Nuclear reactions induced by stable WBPs provide good-quality fusion data and a basic understanding of the underlying reaction physics that would prove reliable information in understanding the future results obtained from radioactive ion beams. Reactions induced by such complex nuclei are manifold in nature. Thus processes like complete and incomplete fusion (ICF), elastic breakup, transfer accompanied by a breakup, and direct stripping or pickup, appear in the reaction dynamics. Figure 1 pictorially describes these processes. The complete merger of the projectile (without breakup) with the target leads to the formation of a compound nucleus (CN) and is termed direct complete fusion. If all the projectile fragments (after breakup) fuse with the target, the process is called sequential complete fusion. The process is called ICF if only one fragment fuses with the target and the others fly away. The ICF competes in heavy-ion collisions with the quasi-elastic reactions, such as the direct transfer of nucleons and non-capture breakup, which happens with less energy loss [4–6]. Furthermore, the interplay of ICF and CF in WBP-induced reactions provides insight into the couplings that occur from breakup and transfer processes, along with some information on the impact of the dissipative environment at energies near the barrier. Enhanced breakup and transfer processes result from the weak binding and clustering in WBP nuclei, especially in the vicinity of the barrier [3].

The strength of ICF over CF for cluster-structured nuclei (^{6,7}Li, ^{9}Be, ^{12,13}C, ^{16}O, and ^{19}F) and its dependence on different entrance channel parameters have been studied over the past few years within the ≈3–10 MeV/nucleon energy range [7–10]. The ICF strength function F_{ICF} has been found to vary linearly with the target charge Z_t, and with the incident projectile energy E_{lab} [7, 11]. However, Zhang *et al* reported that the model-independent ratio of ICF with total fusion (TF) (σ_{ICF}/σ_{TF}) is inversely related to the projectile energy below the Coulomb barrier energies, and an average value of ≈32% at above barrier energies exist for ^{9}Be+^{181}Ta system [4]. In a recent study, Chauhan *et al* [12] discussed the reaction dynamics of ^{7}Li+^{181}Ta (up to 6.5 MeV/nucleon energy). They indicated the presence of ICF or transfer followed by ICF in the α-emitting channels. The partial fusion of a fragment happens when in the non-central/peripheral collisions, the driving input angular momenta exceed the critical limit ℓ_{crit} for CF, and the potential pocket vanishes, restricting the capture of the entire projectile. In such an event, the projectile promptly emits a fragment from itself (P^{s}: spectator) in order to release the excess input angular momenta, and the remnant part (P^{r}) fuses with the target [13].

In the last decade, much attention has been paid to fusion suppression with respect to the coupled-channel calculations or the uni-dimensional barrier penetration model predictions in reactions caused by ^{6,7}Li projectiles on various mass targets [3, 14–16]. A CF suppression of around ≈13%–35% have been observed for ^{6}Li reactions on ^{64}Ni [17], ^{90}Zr [18], ^{96}Zr [19], ^{124}Sn [20], ^{144}Sm [21], ^{152}Sm [22], ^{159}Tb [23], ^{197}Au [24], ^{198}Pt [6], ^{208}Pb [15], and ^{209}Bi [25]. Contrary to the accepted pattern of CF suppression growing with target mass, Kumawat *et al* [18] argued the presence of a universal suppression factor of about 30% for CF of a ^{6}Li projectile with various targets at above barrier energies. The reason for such CF suppression is the weakly bound nature of ^{6,7}Li, which kicks off other processes like ICF, elastic breakup, and transfer, along with CF. To establish more clarity on these coexisting processes, we measured the evaporation residue cross section for ^{6}Li+^{181}Ta reaction in the 4.5–7.1 MeV A^{-1} energy range and tried to disentangle the reaction dynamics involved. It has

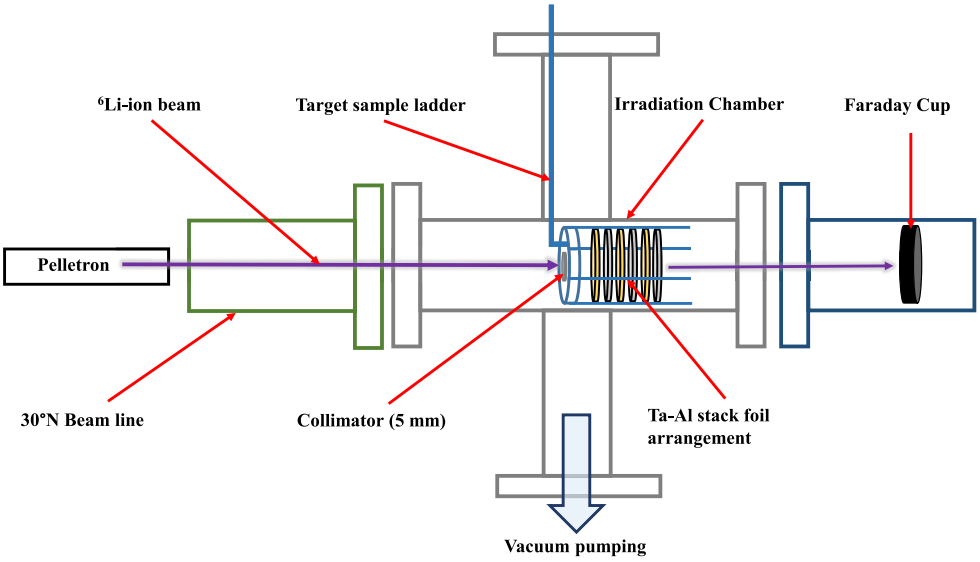

Figure 2. A schematic diagram of the experimental layout employed to study the ^{6}Li $+^{181}$Ta reaction.

been a continuous effort of our group to quantitatively explain the reaction dynamics of ^{6,7}Li on targets with varying masses like ^{nat}Cu [26, 27], ^{89}Y [11, 28], ^{93}Nb [7], ^{nat}Mo [29], ^{nat}Zr [30], and ^{nat}Ta [12].

The article presents a detailed study of the reaction mechanism and the contribution of ICF in the ^{6}Li+^{181}Ta system within the 27–43 MeV energy range. Sections 2 and 3 offer experimental details and a summary of the theoretical calculations. Following a discussion of the study's findings in section 4, section 5 wraps up the report.

2. Experimental details

A ^{6}Li-ion beam with a maximum energy of 43 MeV was used for the experiment performed at the 14 UD BARC-TIFR Pelletron Accelerator facility in Mumbai, India. Self-supporting thin foils of natural ^{181}Ta of 1.4–2.4 mg cm^{-2} thickness and Al-foils of 1.6–1.9 mg cm^{-2} thickness were prepared by rolling technique using spectroscopically pure (99.99%) tantalum (isotopic abundance: ^{181}Ta = 99.988% and ^{180m}Ta = 0.012%) and aluminum (^{27}Al) metal foils. Four Ta–Al stacks, each containing three Ta foils and three Al-foils arranged in an alternative fashion, were irradiated by ^{6}Li^{3+}-ions with varying incident energy. As a result, there were enough energy points between the two subsequent irradiations. The Al-foils served as an energy degrader and a catcher for recoiling heavy residues in the beam direction. A layout of the experimental setup is shown in figure 2, demonstrating the passage of the beam through the stack foil arrangement. The intensity of the incoming beam flux and half-lives of the anticipated residues were considered in deciding the duration of irradiation. Energy degradation of ^{6}Li ions in each foil of a stack was estimated by Stopping and Range of Ions in Matter (SRIM) code [31], and the typical energy losses in the Ta targets used were found to be ≈0.35–0.5 MeV and that in the Al catcher foils were ≈0.4–0.57 MeV in the studied energy range. The projectile energy is taken as an average of the incident and outgoing beam energy. An almost constant beam current (≈11 pnA) was maintained during the experiment, and an

Table 1. Nuclear spectroscopic data of the residues produced in the ^{6}Li+^{181}Ta reaction. The γ-ray energies marked in bold have been used for the cross section calculation.

Residue	J^{π}	Half-life	Decay mode (%)	$E\gamma$ (keV)	$I\gamma$ (%)	Reaction	E_{th} (MeV)
^{183g}Os [35]	$9/2^{+}$	13.0 h	EC[a] (100)	**114.43**	21.1	^{181}Ta(^{6}Li, 4n)	23.74
				167.85	9.0		
				381.74	91.6		
				851.46	4.66		
^{183m}Os [35]	$1/2^{-}$	9.9 h	EC (85), IT[b] (15)	1034.68	6.0	^{181}Ta(^{6}Li, 4n)	23.74
				1101.94	49.2		
				1107.92	22.3		
^{182}Os [34]	0^{+}	21.84 h	EC (100)	**130.8**	3.3	^{181}Ta(^{6}Li, 5n)	31.1
				180.2	34.1		
				263.29	6.76		
^{183}Re [35]	$5/2^{+}$	70.0 d	EC (100)	**162.33**	25.1	^{181}Ta(^{6}Li, p3n)	20.71
^{183}Ta [35]	$7/2^{+}$	5.1 d	β^{-} (100)	**246.06**	27.2	^{181}Ta(^{6}Li, 3pn)	19.63
				353.99	11.6		
^{182m2}Ta [34]	10^{-}	15.84 min	IT (100)	**146.78**	36.5	^{181}Ta(^{6}Li, αp)	0.0
				171.57	48.0		
^{180}Ta [34]	1^{+}	8.154 h	EC (85), β^{-} (15)	**93.32**	4.51	^{181}Ta(^{6}Li, αp2n)	11.65

Notes.
[a] Electron capture.
[b] Isomeric transition.

electron-suppressed Faraday cup housed at the rear of the target assembly (see figure 2) measured the total charge deposited in each irradiation (average total dose ≈250 μC).

After irradiation, the induced activity in each Ta–Al (target–catcher) assembly was assayed using γ-ray spectrometry at regular intervals for a sufficient time with the help of a high-purity germanium (HPGe) detector, which was pre-calibrated using the standard sources, ^{152}Eu (13.506 y), ^{137}Cs (30.08 y), and ^{60}Co (5.27 y) of known activity. Detector resolution of 2.0 keV was estimated in the γ-ray peak at 1332 keV of ^{60}Co. The populated residues were identified using characteristic γ-rays and decay profiles obtained from the recorded spectra. Background-subtracted peak area counts of particular γ-ray energy were used to evaluate the experimental yield [32]. The cross section of a residue, $\sigma(E)$, at an incident energy E, is evaluated using the activation formula [33]

$$\sigma(E) = \frac{\lambda C(t) e^{\lambda T_w}}{\varepsilon^{\gamma} I^{\gamma} A_{tg} \phi (1 - e^{-\lambda T_i})(1 - e^{-\lambda T_a})}, \quad (1)$$

where $C(t)$ is the area counts under the photo peak, λ is the decay constant of the radionuclide under consideration, ε^{γ} and I^{γ} are the geometry-dependent efficiency of the detector and branching intensity of the characteristic γ-ray of the residue. A_{tg} is the areal density of the target atoms, ϕ corresponds to the beam flux, T_w, T_i and T_a represent the cooling or waiting time, irradiation time and acquisition time, respectively. Table 1 reports the nuclear spectroscopic data of the residues [34, 35] formed in the ^{6}Li+^{181}Ta reaction. This information was used to identify and calculate the cross sections of these residues using equation (1).

The following intrinsic uncertainties may exist in the cross section measurement: (i) 2% measurement error in the geometry-dependent efficiency of the detector, (ii) target non-uniformity results in a 2% measurement error for the target thickness, (iii) fluctuations in the beam current could lead to uncertainty in the beam flux of around 7%, (iv) although deadtime was maintained under 8%, statistical uncertainty in the peak counts may propagate error in the cross section measurement, (v) error in beam energy estimation caused by energy deterioration as the beam passes through successive target foils; however, energy straggling effects are not expected to be significant here [36]. The cumulative effect of all the mentioned uncertainties led to an average estimated error of ≈11%, while in a few instances where counting statistics were poor, it increased to ≈21%. An error arising in the SRIM calculation and assessment of the target thickness are two sources of uncertainty that are included in the error estimation of the incident projectile energy for each foil.

3. Model calculation

The complex nature of the nuclear reactions at low energies makes it customary to employ both experimental data with theoretical predictions to gain a thorough understanding of it. Thus, we have used two nuclear reaction model codes: PACE4 [37] and EMPIRE-3.2.2 [38], to study the measured cross sections of the residues formed in the ^{6}Li+^{181}Ta reaction. Both the model codes have been briefly discussed here.

PACE4 comes preinstalled in the framework of LISE++ and is based on the Hauser-Feshbach (HF) formalism of compound nuclear decay. It follows a correct procedure of angular momentum coupling at each stage of deexcitation of excited nuclei. This helps in monitoring the angular distribution of evaporated particles at each stage of deexcitation. The optical model potential is used to obtain the transmission coefficients for light particle (n, p, α) emissions [39]. PACE4 uses the Bass model to estimate the fusion cross section and initial spin distribution for the heavy projectile [40]. The level density parameter in this model is calculated from the expression $a = A/K$, where A is the compound nucleus mass number, and K is a free parameter, $K = 9$ has been used in the calculations for the present reaction. The ratio of the Fermi–Gas level density parameter 'a' at the saddle point to the ground-state value, denoted as ARATIO, has been taken as unity in the calculations. Since PACE4 is a Monte-Carlo code, a total of 100 000 events were used in our calculation. Quantum mechanical treatment of transmission probabilities in the framework of Hill and Wheeler [41] approach has been ensured.

Specifically created for calculations over a wide range of energies and incident particles, EMPIRE-3.2.2 [38] is a multifunctional nuclear reaction algorithm that combines all three basic reaction processes—equilibrium (EQ), pre-equilibrium (PEQ), and direct (DIR) into its formalism. EMPIRE has been tasked with describing the reaction mechanism of the ^{6}Li+^{181}Ta reaction. It utilizes a statistical formulation that combines the EQ and PEQ models to determine the cross section of residues precisely. It contains the HF model with width fluctuations correction for EQ processes, whereas the Exciton model handles PEQ processes. Direct reactions have been accounted for using the coupled channels (CC) and distorted-wave Born approximation approach. Additionally, the coupled-channel code [42], which incorporates the inelastic excitations of the interacting partners and transfer reaction channels independently, has been used to evaluate the heavy-ion fusion cross section. Exciton model with a mean free path parameter value of 1.5 and HF formalism have been utilized to estimate the PEQ and EQ cross sections of the residues, respectively, to explain our current findings. An optical model has been used to derive the transmission coefficients of particle emissions, a

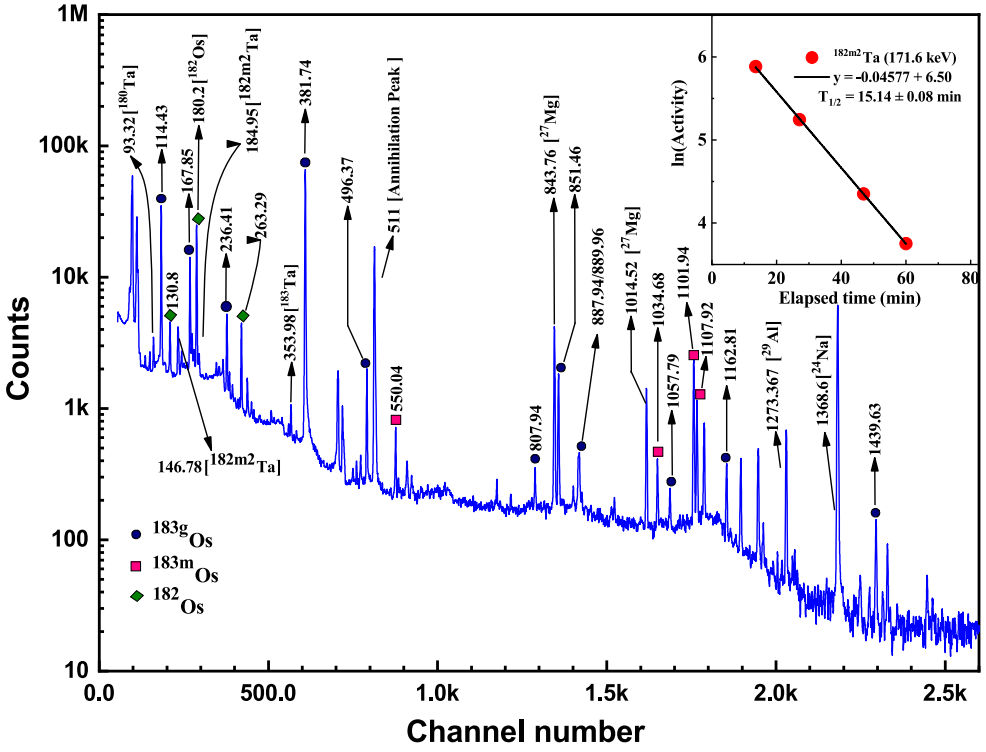

Figure 3. A typical γ-ray spectrum of a ^{181}Ta target, exposed to a 43 MeV ^{6}Li beam, was obtained 22.0 min after the EOB. In the spectrum, the displayed γ-ray energies are in keV. The inset shows the decay curve analysis of ^{182m2}Ta.

crucial component in the cross section computations. The optical model parameters for the neutron and proton were obtained from the global systematics of Koning and Delaroche [43], those for the deuteron from Haixia *et al* [44], those for the triton and ^{3}He from Becchetti and Greenless [45], and those for the alpha particles from Avrigeanu *et al* [46].

In order to estimate the cross section of residues produced in any nuclear reaction, level density models are needed. The Gilbert–Cameron model (GC), Generalized Superfluid model (GSM), and Enhanced Generalized Superfluid model (EGSM) level densities have been used inside the EMPIRE framework to assess the overall impact and significance of level density on the underlying reaction mechanism. Each of the three models is primarily based on the Fermi Gas model (FGM) and treats the same in distinct energy regimes. A detailed discussion of these models can be found in [27].

4. Results and interpretation

The ^{6}Li+^{181}Ta reaction produced ^{183m,183g,182}Os, ^{183}Re, and ^{183,182m2,180}Ta residual radionuclides via various reaction channels within the 27–43 MeV incident energy range. These radionuclides are shown in figure 3 with their characteristic γ rays at the maximum incident energy of 43 MeV. Table 1 lists the most likely reaction pathways that could result in the generation of these residues, along with the related reaction thresholds. Table 2 reports the cross section of the evaporation residues at various energies, and it can be noted that the *xn*

Table 2. Cross sections (mb) at different incident energies of evaporation residues formed in the ^{6}Li+^{181}Ta reaction.

Energy (MeV)	Cross sections (mb)						
	^{183g}Os	^{183m}Os	^{182}Os	^{183}Re$_{cum}$	^{183}Ta	^{182m2}Ta	^{180}Ta
27.2 ± 0.6	0.3 ± 0.01	—	—	—	—	0.3 ± 0.06	2.5 ± 0.6
28.8 ± 0.7	4.2 ± 0.55	2.4 ± 0.5	—	9.7 ± 3.1	—	0.8 ± 0.2	5.4 ± 1.0
30.2 ± 0.6	23.2 ± 2.8	8.0 ± 1.2	—	31.7 ± 6.8	—	1.1 ± 0.2	6.3 ± 1.4
31.5 ± 0.7	76.9 ± 9.3	18.6 ± 3.0	—	83.7 ± 14.6	—	1.5 ± 0.3	8.1 ± 1.8
32.8 ± 0.7	117.1 ± 13.2	23.6 ± 4.0	—	147.5 ± 25.0	—	1.7 ± 0.3	10.4 ± 1.9
37.8 ± 0.8	325.6 ± 31.3	56.6 ± 7.0	11.5 ± 2.7	468.8 ± 124.6	—	3.6 ± 1.1	11.4 ± 2.5
39.0 ± 0.8	395.6 ± 37.9	59.4 ± 7.2	37.9 ± 5.5	492.2 ± 123.2	—	2.8 ± 0.9	14.8 ± 1.8
40.2 ± 0.9	360.1 ± 34.4	58.4 ± 7.2	87.0 ± 10.9	526.6 ± 154.4	9.4 ± 4.6	2.3 ± 0.6	13.9 ± 2.7
41.5 ± 0.9	337.5 ± 32.3	56.6 ± 7.2	156.0 ± 17.7	559.1 ± 139.9	29.1 ± 5.8	2.2 ± 0.4	13.4 ± 2.7
42.8 ± 0.9	337.6 ± 32.3	55.0 ± 7.0	266.7 ± 28.8	572.0 ± 122.9	35.2 ± 5.8	2.4 ± 0.4	14.9 ± 2.8

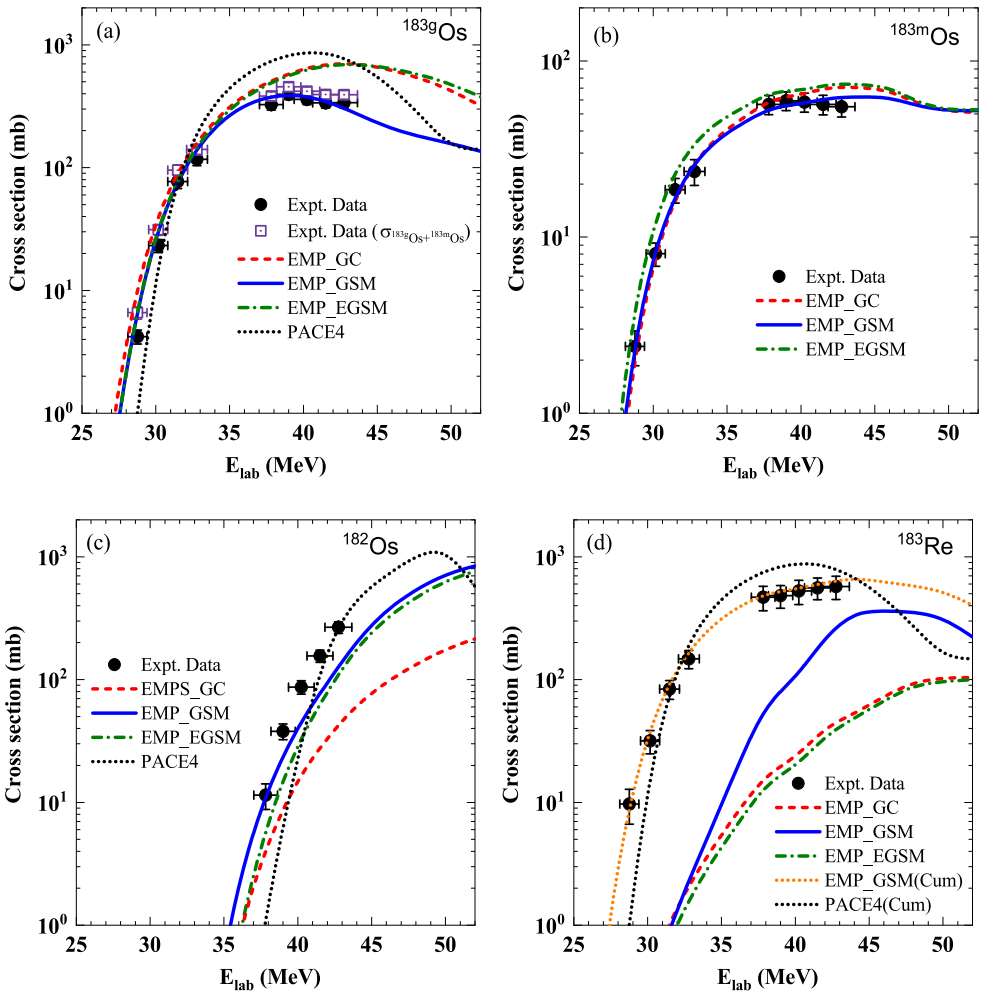

Figure 4. Experimental excitation functions (solid black circles) of *xn* channel residues: (a) ^{183g}Os, (b) ^{183m}Os, (c) ^{182}Os, and *pxn* channel residue: (d) ^{183}Re from ^{6}Li+^{181}Ta reaction are compared with those obtained from theory using EMPIRE with GC (red dashed curve), GSM (solid blue curve), and EGSM (green dashed-dotted curve) level density and PACE4 (black dotted curve).

and *pxn* channel residues show dominant cross sections, especially ^{183g}Os and ^{183}Re$_{cum}$. In figures 4 and 5, the experimental excitation functions of the residues are compared with the theoretical predictions of EMPIRE-3.2.2 [38] and PACE4 [37]. Experimental data are depicted by symbols with associated errors, whereas lines represent the theoretical calculations.

Figure 4 displays the excitation functions for residues populated through the *xn*- and *pxn* channel. The experimental excitation function for ^{183g}Os is compared with the ones predicted by EMPIRE and PACE4 in figure 4(a) where it can be seen that experimental cross sections reach a maximum value of 395.6 ± 37.9 mb (see table 2). The measured cross sections (black filled circle) at energies below 35 MeV are accurately reproduced by calculations with EMPIRE considering three different level densities (GC, GSM, and EGSM), and GSM (see solid blue curve) has better predictability than the other two level densities above 35 MeV.

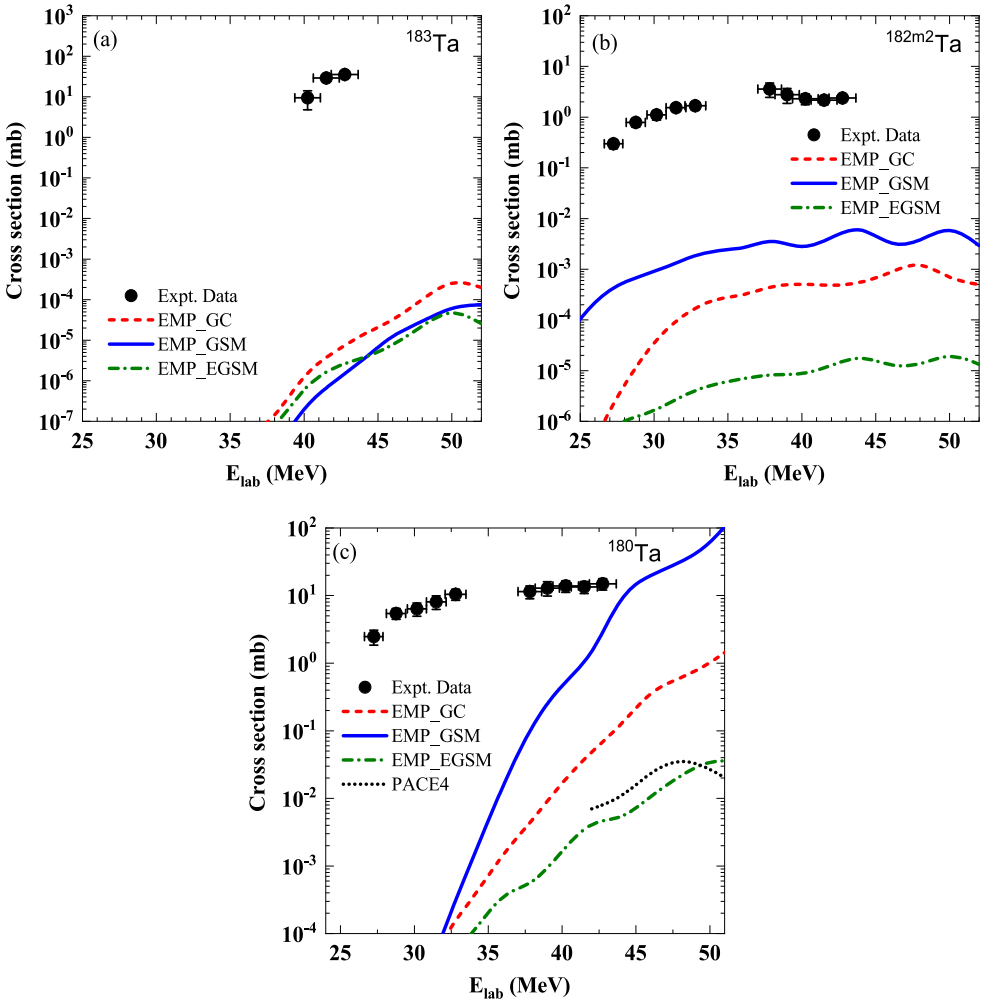

Figure 5. Same as figure 4 but for (a) ^{183}Ta, (b) ^{182m2}Ta, and (c) ^{180}Ta populated through the 3*pn* and αpxn channels.

The GC and EGSM level density overpredicts the data at higher energies (∼6–8 MeV/nucleon). Since PACE4 does not provide cross sections for isomers, instead gives the total cross sections (i.e. the sum of ground and metastable state), we have compared PACE4 predictions with total cross sections of ^{183}Os (see purple open squares in figure 4(a)). It is noteworthy that PACE4 (black dotted curve) predicts a similar trend of cross sections as the measured ones and the EMPIRE calculated ones. However, the lower energy regime ($E_{lab} <$ 35 MeV) seems to underpredict the data slightly. PACE4 matches the experimental cross sections at two energy points near 35 MeV but markedly overpredicts at higher energies (>35 MeV). Similarly, for ^{183m}Os (metastable state) produced by ^{181}Ta(^{6}Li,4n) reaction, the experimentally obtained cross sections in the 27–43 MeV energy range shown in figure 4(b) are predicted well with the EMPIRE calculations employing all three level densities. Here we observe that the cross sections obtained using all three level densities lie in close proximity with the experimental data as well as each other; however, the GSM-calculated ones are more

accurate. PACE4 is unable to predict the isomeric state cross sections separately, hence not shown in figure 4(b).

Figure 4(c) shows the excitation functions for ^{182}Os (obtained via 5*n* channel) and depicts the fact that the cross sections provided by EMPIRE choosing GSM and EGSM level density to lie much closer to the experimental data compared to the GC; however, they still slightly underpredict the data. The GSM calculations predict cross sections closer to the data at the lowest energy points but deviate minutely as the energy increases. Moreover, PACE4 predicts cross sections lower than the experimental ones at energies lower than 40 MeV but satisfies the data at energies above 40 MeV. ^{183}Re is produced via the proton emitting channel ($p3n$) from the ^{6}Li+^{181}Ta reaction. Its excitation function is displayed in figure 4(d), which shows an overall enhancement of the measured cross sections over the model-calculated ones. This enhancement can be attributed to the fact that the measured cross sections of ^{183}Re are cumulative and is a consequence of two processes, (a) the direct population through the $p3n$ decay channel from the compound nucleus ^{187}Os*, and (b) the activity induced by the decay of higher charge isobars known as parent radionuclide, ^{183g}Os ($T_{1/2}$= 13.0 h) 100% EC to ^{183}Re ($T_{1/2}$= 70.0 d) and ^{183m}Os ($T_{1/2}$= 9.9 h) 85% EC to ^{183}Re (daughter radionuclide). Theoretical cumulative production cross sections of ^{183}Re are calculated keeping in mind the method proposed by Cavinato *et al* [47] and compared with experimental data in figure 4(d) (here shown calculation only for EMPIRE with GSM level density and PACE4). It reveals that the calculations of EMPIRE considering GSM level density reproduce the cumulative cross sections satisfactorily in the whole energy range. However, one can also note that PACE4 does not agree with the data well, underpredicting it below 35 MeV and overpredicting it above it. It is worth noting that there is a general agreement of the EMPIRE model calculations as compared to PACE4 with the experimental data of residues formed from the *xn* and *pxn* channels, except for the ^{182}Os, which showcases a slight deviation. This implies that the reaction mechanism involved in forming these residues corresponds to a mixture of compound nuclear and PEQ processes since an EQ + PEQ mechanism is used in the EMPIRE model calculations.

Figure 5 illustrates the excitation functions of ^{183}Ta, ^{182m2}Ta, and ^{180}Ta residues produced through the decay of ^{187}Os* CN from 3*pn* and αpxn channels, where $x = 0$ and 2. The comparison of experimental cross sections of ^{183}Ta (3*pn* decay channel) with the EMPIRE calculated ones are displayed in figure 5(a), which brings out an observation that the experimental data is about 4 to 5 orders of magnitude higher than the model-predicted ones. PACE4 fails to predict any cross section for this residue. Similarly, for the case of ^{182m2}Ta (αp decay channel), we observe (see figure 5(b)) that the experimental cross sections lie 3 to 4 orders of magnitude higher than EMPIRE calculations with GSM level density and much more compared to the other two level density options. It can be noted that the EMPIRE model with different level densities predicts cross section in the ten nb to a few μb range. For ^{182}Ta too PACE4 fails to predict any cross section in the studied energy range. Furthermore, if we shed our focus on figure 5(c), which depicts the excitation function of ^{180}Ta residue ($\alpha p2n$ decay channel), we observe an enhancement in the measured cross sections over the theoretical estimates. The GSM level density calculated cross section tends to approach the experimental ones towards the higher energy side, whereas the EGSM and GC level density sharply underpredict the data over the measured energy range (27–43 MeV). We also observe sharp underprediction of cross section by PACE4 but they are close to the EMPIRE calculated ones considering EGSM level density. Hence, looking at figures 4 and 5, we can conclude that EMPIRE is better in predicting the cross sections of the residues as compared to PACE4, and the fundamental reason could be the underlying reaction mechanism that they follow. EMPIRE

Table 3. Details of the different possible CF and ICF channels in the ^{6}Li+^{181}Ta reaction.

CF of ^{6}Li		ICF of ^{6}Li (^{6}Li $\rightarrow \alpha + d$)	
Reaction	Q-value (MeV)	Reaction	Q-value (MeV)
^{181}Ta(^{6}Li, 4n)^{183g}Os	−22.97	^{181}Ta(α, 2p)^{183}Ta	−15.3
^{181}Ta(^{6}Li, 4n)^{183m}Os	−22.97	^{181}Ta(α, 2np)^{182m2}Ta	−22.23
^{181}Ta(^{6}Li, 5n)^{182}Os	−30.1	^{181}Ta(α, αn)^{180}Ta	−7.58
^{181}Ta(^{6}Li, p3n)^{183}Re	−20.04	^{181}Ta(d, p)^{182m2}Ta	3.84
^{181}Ta(^{6}Li, 3pn)^{183}Ta	−18.99	^{181}Ta(d, p2n)^{180}Ta	−9.8
^{181}Ta(^{6}Li, αp)^{182m2}Ta	2.36		
^{181}Ta(^{6}Li, αp2n)^{180}Ta	−11.28		

works on the EQ+PEQ mechanism, whereas PACE4 only takes into account the EQ phenomenon in its framework.

Finally, keeping in mind the facts presented above, it is worth mentioning that an overall enhancement in the total cross sections of residues observed from the 3*pn* and αpxn channel exists over EMPIRE calculations with HF formalism for EQ and exciton model for PEQ. Thus, the excess cross sections are inherent to the third variety of reaction processes which is not considered in the model calculations. A possible candidate is the breakup fusion and/or massive transfer-like processes, generally characterized under incomplete fusion (ICF). ICF processes are quite probable in reactions involving weakly bound nuclei. There is a reasonable chance that the weakly bound ^{6}Li ($\alpha + d$) might breakup directly; ^{5}Li and ^{8}Be could breakup directly into $\alpha + p$ and $\alpha + \alpha$, respectively, after a nucleon transfer between ^{6}Li and the target within ∼3–7 MeV/nucleon energy range as proposed by numerous experimental studies [6, 48]. Therefore, the mixture of the CF and ICF processes outlined below may cause the large production cross sections of ^{183,182m2,180}Ta.

CF: The complete mass amalgamation of ^{6}Li in ^{181}Ta leads to the formation of ^{187}Os* CN in an excited state. The deexcitation of this CN through the emission of light particles (e.g. *n*, *p*, α) eventually produces residual nuclei (table 3).

ICF: The ^{6}Li projectile may dissociate into an α particle and a deuteron (*d*) in the nuclear force field of ^{181}Ta owing to its low breakup threshold (1.47 MeV). One of the newly formed partitions can fuse with the Ta target to form a reduced compound nucleus in an excited state, while the remaining one departs away in the forward direction as a spectator. An answer to the large production cross sections of ^{183,182m2,180}Ta residues could be the ICF or nucleon transfer processes in the ^{6}Li+^{181}Ta reaction. The possible scenarios follow accordingly:

(1) The fusion of α-particle (a post-breakup product of ^{6}Li) with ^{181}Ta leads to the formation of ^{185}Re*, which after the emission of an α and some neutrons may produce ^{183,182m2,180}Ta (table 3) while the *d* happens to move in the initial projectile direction with proportional velocity. Likewise, the fusion of *d* (*d*-ICF) may lead to the formation of ^{183,182m2,180}Ta via the *pxn* channel (refer to table 3). In comparison to the α-capture route, the *d*-capture route is more favorable for the formation of ^{182m2}Ta due to the positive Q-value for the reaction, whereas for ^{183,180}Ta, the α-capture is more suitable because of a low Q-value.

(2) A definite possibility of one-neutron stripping from ^{6}Li to ^{181}Ta exists, which produces ^{182}Ta* (or ^{182m2}Ta) and ^{5}Li, which happens to dissociate into $\alpha + p$. For the neutron transfer reactions, ^{181}Ta(^{6}Li, ^{5}Li $/(\alpha + p)$)^{182}Ta, the Q-values are +0.4 MeV for ^{5}Li as

product and +2.364 MeV for $\alpha + p$. Thus, a strong possibility of neutron transfer events followed by a breakup is manifested in the presence of positive Q-values; Zhang *et al* [49] demonstrated the presence of $1n$-stripping from ^{6}Li to ^{89}Y and reported their cross section explicitly. $1n$-stripping has also been shown as a major process in ^{6,7}Li+^{197}Au reactions [5, 24].

(3) One-proton stripping [50] has been reported to contribute to the reaction mechanism involving ^{6}Li. Thus, one-proton stripping from ^{6}Li to ^{181}Ta leads to the formation of ^{182}W* and ^{5}He, which tends to break up into $\alpha + n$. The populated ^{182}W* can then subsequently decay via either emission of particle or gamma, and the likely reaction would be $^{6}\mathrm{Li} + {}^{181}\mathrm{Ta} \rightarrow {}^{5}\mathrm{He} + {}^{182}\mathrm{W}^{*}$ ($Q = +2.663$ MeV) or $\rightarrow \alpha + n + {}^{182}\mathrm{W}^{*}$ (Q = +3.4 MeV). However, Castaneda *et al* [51] demonstrated that roughly 50% of inclusive α can be related to production via $^{6}\mathrm{Li} \rightarrow \alpha + d$ and $^{6}\mathrm{Li} \rightarrow {}^{5}\mathrm{He} \rightarrow \alpha + n$ exclusive breakup channels in the ^{6}Li+^{197}Au system. They assumed the $1p$-stripping followed by breakup $^{6}\mathrm{Li} \rightarrow {}^{5}\mathrm{He} \rightarrow \alpha + n$ cross sections to be equivalent to $1n$-stripping followed by breakup $^{6}\mathrm{Li} \rightarrow {}^{5}\mathrm{Li} \rightarrow \alpha + p$.

(4) There might be a chance of one-neutron pickup by ^{6}Li from ^{181}Ta, leading to the formation of ^{180}Ta*. The large enhancement in the ^{180}Ta ER cross section might be a consequence of this direct transfer process which happens to have a finite possibility of taking place, as reported by Shrivastava *et al* [52] for the ^{6}Li+^{65}Cu reaction.

(5) Another possibility remarked by Shrivastava *et al* [52] is triton-stripping. One triton-stripping from ^{6}Li to ^{181}Ta leads to the formation of ^{184}W* and ^{3}He. The populated ^{184}W* can then decay via particle or gamma emission to form ^{183,182m2,180}Ta residues. Although the ground-state Q-value for $^{181}\mathrm{Ta}(^{6}\mathrm{Li}, {}^{3}\mathrm{He})^{184}\mathrm{W}^{*}$ is -3.57 MeV, the reaction would depend upon the optimum Q-value for this transfer process.

With so many possibilities of different processes entering into the reaction mechanism of ^{6}Li+^{181}Ta, it is desirable that these processes should be added to the framework of the EMPIRE model code. EMPIRE has a modular structure, with different modules performing a well-defined task and communicating with other modules through a set of global COMMONS, which are included in most subroutines. This feature assures access to all the resources throughout the code and facilitates adding new features and mechanisms. This opens a window of improvement in the EMPIRE code where the breakup fusion or ICF mechanism can be added to its formalism without compromising its present capabilities. It can be mentioned here that some models like the break-up fusion model [53] and the SUMRULE model [54] do exist to explain the ICF dynamics in heavy-ion induced reactions. However, these models can correctly predict the magnitude of ICF for some cases at energies $\geqslant$10 MeV/nucleon, none of these is able to successfully explain the ICF data at energies $\approx$4–7 MeV/nucleon. The proper integration of such models into the EMPIRE code can be attempted to explain ICF, which would boost the capabilities of this code to universally simulate the reaction mechanism for a wide variety of target-projectile combinations.

4.1. Incomplete fusion analysis

Since we have measured the production cross sections of various populated evaporation residues in the ^{6}Li+^{181}Ta reaction using the γ spectrometric method, the determination of the ICF cross section is heavily dependent on models rather than only from the experiment. An enhancement in the cross sections of ^{183,182m2,180}Ta has been observed over the EMPIRE estimations, as shown in figure 5. Since ICF or transfer followed by ICF is not considered by EMPIRE in its formalism, the residues are assumed to be populated purely via the CF mechanism in the ^{6}Li+^{181}Ta reaction. To showcase the behavior of ICF better, the sum of

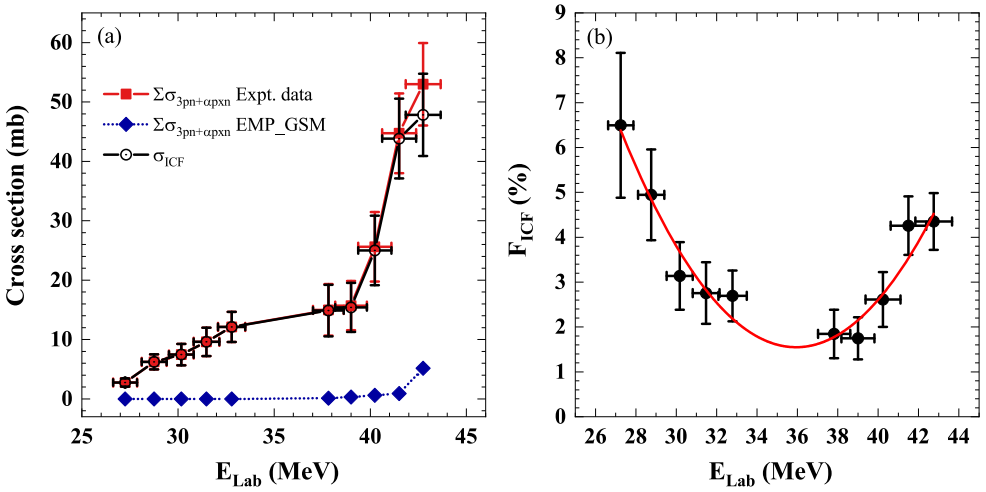

Figure 6. (a) CF, ICF, and TF cross sections for α-emitting channels as a function of projectile energy and (b) variation of $F_{\rm ICF}$ (ICF strength function) with incident projectile energy. The solid line is to guide the eye.

experimentally measured cross sections of α-emitting channels ($\Sigma\sigma_{\rm expt}^{3pn+\alpha pxn}$) have been compared with those predicted by EMPIRE with GSM level density ($\Sigma\sigma_{\rm EMPIRE}^{3pn+\alpha pxn}$) and are shown in figure 6(a). The total measured cross sections for α-emitting channels is significantly higher than the sum of cross sections estimated by EMPIRE calculations taking the same input parameters into account, which were able to reproduce the *xn* and *pxn* channel residues cross sections, which are primarily populated from CF mechanism. Henceforth, the observed enhancement in the measured cross section of α-emitting channels is chiefly a result of the contribution from ICF and nucleon transfer followed by ICF processes. In view of this fact, the ICF strength function has been deduced using the data reduction method [7, 55].

To quantify the amount of ICF contribution in the ^{6}Li+^{181}Ta reaction, the ICF cross section ($\sigma_{\rm ICF}$) has been calculated as $\Sigma\sigma_{\rm ICF} = \Sigma\sigma_{\rm TF}^{3pn+\alpha pxn} - \Sigma\sigma_{\rm CF}^{3pn+\alpha pxn}$, where $\sigma_{\rm TF}$ and $\sigma_{\rm CF}$ represent the sum of experimental and theoretical cross sections, respectively, and $x = 0$ and 2. Figure 6(a) shows the $\sigma_{\rm TF}$ (red line with square symbols), which is the sum of measured cross sections of ^{183}Ta, ^{182m2}Ta, and ^{180}Ta residue, $\sigma_{\rm CF}$ (blue line), the sum of theoretical cross sections of these three residues obtained from EMPIRE, and $\sigma_{\rm ICF}$ (black line with open circles) denoting the ICF cross sections. The estimated ICF cross section is a model-dependent quantity because of the method used. To understand the extent of the ICF contribution over CF in the α-emitting channel and how it varies with incident energy, ICF fraction ($F_{\rm ICF}$) has been deduced. The ICF fraction (in %) is defined as $F_{\rm ICF} = (\Sigma\sigma_{\rm ICF}/\sigma_{\rm TF}^{\rm theory}) \times 100$, where $\sigma_{\rm TF}^{\rm theory}$ is the total fusion cross section computed theoretically by EMPIRE. The F_{ICF} has been plotted as a function of incident energy in the lab frame in figure 6(b). The behavior of the ICF strength function is intriguing as it shows a parabolic nature with a minimum of ≈36 MeV. A maximum value of ≈6% is found at 27 MeV energy. The increase of F_{ICF} with decreasing incident projectile energy has been reported previously by Zhang *et al* and Dasgupta *et al* for another WBP ^{9}Be in reactions with ^{181}Ta [4] and ^{208}Pb [15], respectively. Also, direct transfer processes around the Coulomb barrier have been shown to compete heavily with the ICF mechanism in reactions with ^{6,7}Li projectiles [6, 48].

Table 4. Potential parameters used in the CRC calculations for the ^{6}Li+^{181}Ta system. V_R, r_R, and a_R are depth, radius, and diffuseness parameters, respectively, of the real volume part of the potential. Similarly, W_V, r_{IV}, and a_{IV} are for the imaginary volume part and W_S, r_{IS}, and a_{IS} are for the imaginary surface part of the optical potential. $R_i = r_i \times A^{1/3}$ where $i = R$, IV, IS, and C.

System	V_R (MeV)	r_R (fm)	a_R (fm)	W_V (MeV)	r_{IV} (fm)	a_{IV} (fm)	W_S (MeV)	r_{IS} (fm)	a_{IS} (fm)	r_C (fm)
^{6}Li + ^{181}Ta [57]	15.9	1.25	0.70	6.30	1.05	0.714	4.56	1.25	0.70	1.30
n + ^{181}Ta [58]	50.0[a]	1.25	0.70	—	—	—	6.0	1.25	0.70	1.25
n + ^{6}Li [59]	50.0[a]	1.25	0.70	—	—	—	6.0	1.23	0.65	1.25

Note.
[a] Depth adjusted to obtain the correct binding energy.

Table 5. Energy levels of transfer products used in coupling scheme of CRC calculations for ^{6}Li+^{181}Ta reaction [34].

^{182}Ta		^{180}Ta	
E (MeV)	J^{π}	E (MeV)	J^{π}
0.0	3^{-}	0.0	1^{+}
0.2704	2^{-}	0.0395	2^{+}
0.4026	2^{+}	0.1107	3^{+}
0.5196	10^{-}	0.3202	1^{+}
		0.3708	2^{+}

Hence, the neutron transfer channels have been investigated using coupled reaction channel (CRC) calculations.

4.2. Coupled reaction channel calculations

In order to comment on the presence of transfer channels, the CRC calculations have been performed using a theoretical model code FRESCO [56]. The recipe for CRC calculations demands essential inputs, such as the optical model potentials for entrance and exit channels, the binding potential between the transferred particle and core nucleus, and spectroscopic factors for different residual states. A Wood-Saxon form of potential has been adopted for real and imaginary parts of the optical potential. Since elastic scattering data has not been measured and is also not present in the literature for the ^{6}Li+^{181}Ta system, the optical model parameters could not be fitted for this specific reaction. Thus, the potential parameters for ^{6}Li+^{181}Ta have been adopted from the work of Figueira *et al* [57], in which an optical model fit to the ^{6,7}Li+^{144}Sm elastic scattering data was performed. These optical model parameters, such as depth, radius, and diffuseness parameters of the real and imaginary parts, are presented in table 4. The binding potential parameters for n+^{181}Ta are the same as those of n+^{208}Pb from [58] because both ^{181}Ta and ^{208}Pb lie in the heavy mass region. Similarly, the n+^{6}Li binding potential parameters are taken from [59] and are tabulated in table 4.

For the 1n-pickup case, the spectroscopic factor (C^2S) for ^{6}Li/^{7}Li has been obtained by shell model calculations using the NUSHELLX code [60]. The p model space (for $1p_{3/2}$ and $1p_{1/2}$ orbitals of ^{6,7}Li) and *ckpot* interaction [61] were used for these calculations. A C^2S value of 0.63 was obtained for the ground-state to ground-state transfer. On the other hand, a C^2S value of 1.12 has been taken for the ^{6}Li/^{5}Li 1n-stripping case from [62]. The spectroscopic factors for the target states in both cases have been assigned a value of 1.0. Among the various states of ^{180}Ta and ^{182}Ta given in [34], those states that actively contribute (with J values less than 5) to the 1n-transfer channels have been included in the coupling scheme and are shown in table 5. In the case of ^{182}Ta, the 10^{-} metastable state ($T_{1/2}$= 15.84 min) has been included in the coupling scheme to estimate the contribution of this state into the reaction cross section. The inelastic states of the projectile (^{6}Li) and the target (^{181}Ta) have not been included in the present calculations. Figure 7 shows the excitation functions of (a) 1n-pickup (^{180}Ta) and (b) 1n-stripping (^{182}Ta) transfer channels in the ^{6}Li+^{181}Ta reaction along with the CRC calculations. It can be observed from figure 7(a) that for the 1n-pickup (^{180}Ta) channel, the CRC calculations (continuous red line) are in excellent agreement with the experimental data. For comparison, the EMPIRE estimations using GSM level density (green dashed line) are also shown, and it can be noted that they highly underpredict the data. However, a few points must be understood for the 1n-stripping (^{182}Ta) case. In the current experiment, the

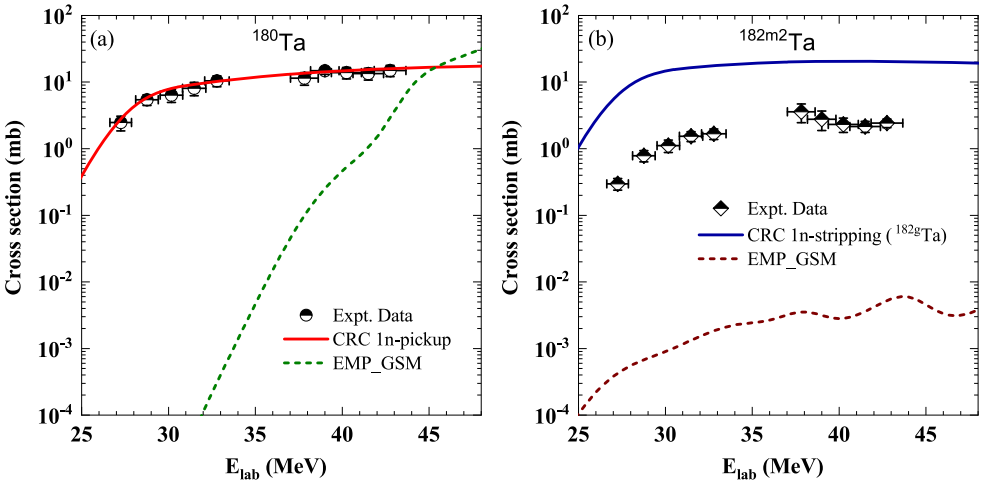

Figure 7. Comparison of the measured excitation functions with CRC calculations (solid curves) of (a) ^{180}Ta (1*n*-pickup) and (b) ^{182m2}Ta (1*n*-stripping) transfer channels in the ^{6}Li+^{181}Ta reaction. The dashed curves are cross sections obtained from EMPIRE calculations shown here to depict the contribution from CF, which is negligible.

ground-state (3^-) of ^{182}Ta could not be unambiguously identified, whereas its metastable (10^-) at 0.52 MeV has been identified, and its cross section is reported. From the CRC calculations, we could find that the ground-state of ^{182}Ta is populated via the ^{181}Ta(^{6}Li,^{5}Li)^{182}Ta 1*n*-stripping channel, whereas the high-spin metastable state (^{182m2}Ta) is not produced through this channel as is evident from figure 7(b). A good reason could be that the population of a high-spin state is rather difficult to achieve in a low-energy nucleon transfer reaction. Thus, as mentioned before, the ^{182m2}Ta residue can be produced via CF or ICF reaction channels.

For comparison of fusion cross sections (σ_{fus}) of reaction induced by ^{6}Li on different mass targets, the σ_{fus} for reaction ^{6}Li+^{197}Au [24], ^{6}Li+^{198}Pt [6], ^{6}Li+^{159}Tb [23], ^{6}Li+^{152}Sm [22], ^{6}Li+^{144}Sm [21] and for the present system have been plotted as normalized cross sections ($\sigma_{fus}/\pi R^2$) as a function of $E_{C.M.}/V_b$ in figure 8, where $R = r_0(A_P^{1/3}+A_T^{1/3})$, A_P, and A_T are the projectile and target masses, respectively; here, a value of $r_0 = 1.2$ fm has been used, and V_b is the Coulomb barrier for a particular system. The fusion cross section for ^{6}Li+^{181}Ta has been estimated as the sum of (i) the experimental cross sections of *xn* and *pxn* channel residues and (ii) the missing cross sections of stable or very short-lived residues of *xn* and *pxn* channel (obtained from EMPIRE-GSM calculations) since the stack foil activation technique limits one to measure these residues. The comparison shows that the normalized fusion cross sections for all the systems are pretty similar except for ^{6}Li+^{144}Sm [21] near the barrier energies (since ^{144}Sm is a spherical nucleus while others are slightly deformed [63]). This comparison also indicates no significant target dependence of the fusion cross sections; similar conclusions have been reported in [15].

4.3. Isomeric cross section ratio

Nuclear isomers are relatively long-lived 'metastable' excited states, with half-lives ranging from nanoseconds to years, and embody a gateway to understanding the structure of the nucleus [64]. A pair of nuclear isomers populated in a reaction can be used to derive the isomeric cross section ratio (ICR). The estimation of ICR provides some crucial details

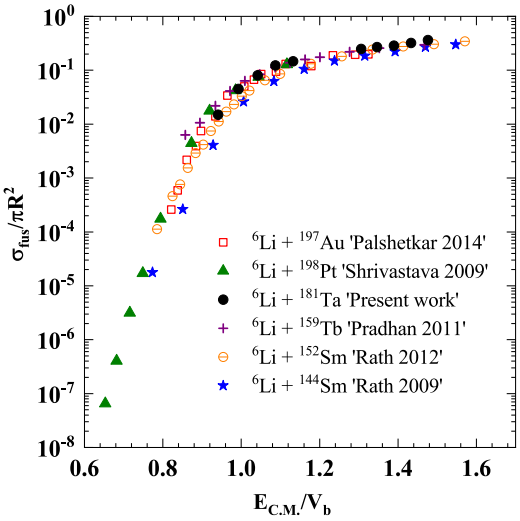

Figure 8. Comparison of normalized fusion cross sections for the present data on ^{6}Li $+^{181}$Ta and ^{6}Li$+^{197}$Au [24], ^{6}Li$+^{198}$Pt [6], ^{6}Li$+^{159}$Tb [23], ^{6}Li$+^{152}$Sm [22], and ^{6}Li $+^{144}$Sm [21] reactions. The quantities $E_{\mathrm{C.M.}}/V_b$ and $\sigma_{\mathrm{fus}}/\pi R^2$ are dimensionless.

regarding the angular momentum change and γ deexcitation that occurs during nuclear decay. The spin of the target nucleus, the projectile's energy, the particle emission, and particularly the spin of the isomeric state affect the value of ICR. To understand the spin population of ^{183}Os, ICR has been computed as the ratio of cross sections of the low-spin ($\sigma_L \equiv \sigma_m$) to the high-spin ($\sigma_H \equiv \sigma_g$) products, ICR $= \sigma_m/\sigma_g$. Figure 9 depicts the associated decay scheme of ^{183m,g}Os, and the evaluated isomeric cross section ratio is shown in figure 10. One can observe that the ICR decreases sharply with increasing ^{6}Li projectile energy and becomes almost constant at energies above 37 MeV. It is possible to comprehend the observed pattern as follows: ^{183}Os residue has a ground-state with spin $9/2^+$ and an isomeric state with spin $1/2^-$ at 0.0 and 170.7 keV, respectively. At low excitation energy, the compound nucleus decays to the low-spin ($1/2^-$) isomeric state, thereby generating more population of ^{183m}Os; however, as the excitation energy increases, the population of the high-spin state ($9/2^+$), that is, the ground-state of ^{183}Os increases. The effect is a fall in the ICR. However, beyond 37 MeV, the composite system emits a vast amount of angular momentum from PEQ emissions, which causes an equilibrium between the two spin states and results in an almost constant ICR [65]. The measured ICR has been compared with one calculated using EMPIRE theoretical code considering the GSM level density in figure 10. It can be noted that the model-predicted values sufficiently agree with the experimentally measured ones over the energy range studied.

5. Conclusion

The article reports the first measurement of the residual cross sections of ^{183m,g}Os, ^{182}Os, ^{183}Re, and ^{183,182m2,180}Ta, from the ^{6}Li$+^{181}$Ta reaction in the 27–43 MeV incident energy range. The measured cross sections have been characterized with the theoretical estimations from EMPIRE-3.2.2 code with EQ and PEQ models and PACE4 (uses only EQ mechanism). The shape of the measured excitation functions confirms the dominance of the equilibrium

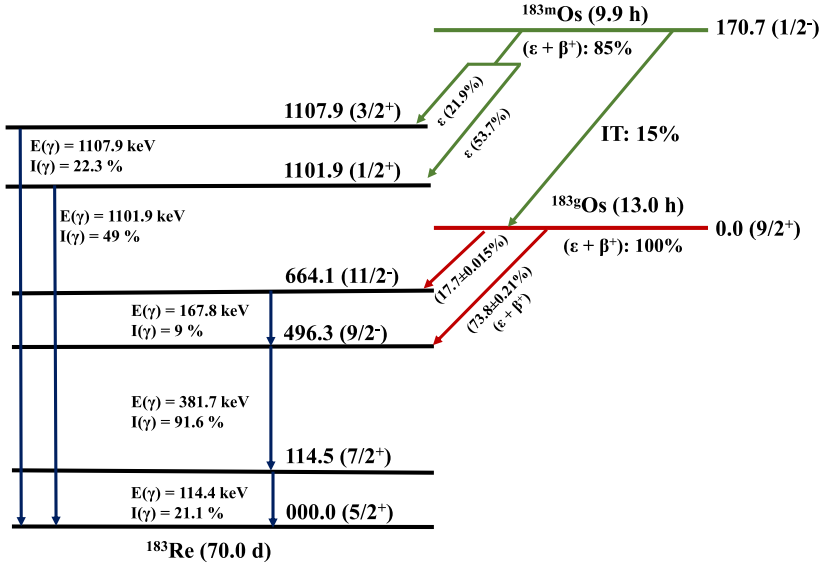

Figure 9. Simplified decay scheme of isomeric pair of ^{183}Os adopted from [35]. Electron capture is denoted by ϵ.

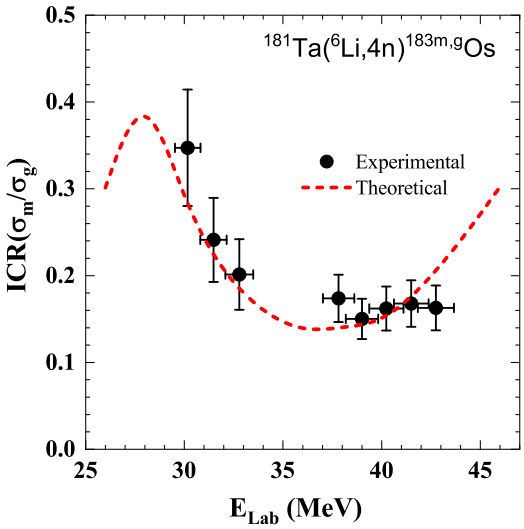

Figure 10. Variation of isomeric cross section ratio (ICR) with the incident energy of the projectile.

mechanism in the *xn* (^{183g,183m,182}Os) and *pxn* (^{183}Re) channel residues; however, a comparison of theoretical calculations with experimental excitation functions for various residues reveals an admixture of the PEQ along with the EQ mechanism. This fact has been confirmed from the observation that EMPIRE outperforms PACE4 in satisfactorily predicting the experimental data. Both PACE4 and EMPIRE computed cross sections show marked deviations from the measured ones in the case of ^{183,182m2,180}Ta residues. This deviation reveals an apparent

enhancement in measured cross sections above the EMPIRE calculations in α-emitting channels, which can be a consequence of either ICF or neutron transfer processes or both entering into the reaction dynamics of the ^{6}Li+^{181}Ta system (since EMPIRE is unable to simulate these processes in its framework). The ICF strength function derived using the data reduction method was found to have a peculiar parabolic shape variation with projectile energy resulting from both ICF and neutron transfer processes above and below E_{lab} = 35 MeV, respectively. CRC calculations (to simulate one-neutron transfer reactions) validate this fact by taking excited states in the transfer products (^{182}Ta and ^{180}Ta) into account. 1n-pickup cross sections are reproduced well with the CRC calculations. Due to the relatively high-spin (10^{-}) of the isomer of ^{182}Ta, its production via the 1n-stripping channel was not observed since such high-spin states are hard to populate via n-transfer at such low energies. The reduced fusion cross sections for ^{6}Li+^{181}Ta have been found to be in good agreement with those for other targets indicating negligible target dependence of the fusion cross sections. Since the ground and isomeric states of ^{183}Os have been populated in the present reaction, ICR has been evaluated from the measured data and compared with that obtained from EMPIRE calculations. A good agreement between the measured ICR and EMPIRE estimation has been reported. ICR has been found to decrease with growing incident projectile energy.

Acknowledgments

We thank the devoted effort of our IIT Roorkee TASISPEC Lab colleagues during the learning period. We acknowledge Research Grant No. 03(1467)/19/EMR-II from CSIR(IN) and the research fellowships (IF180078) from DST-INSPIRE and MHRD(IN), Government of India. We also acknowledge the cooperation from the BARC-TIFR Pelletron staff during the experiment and project No. 12P-R&D-TFR-5.02-0300, Department of Atomic Energy, Government of India.

Data availability statement

All data that support the findings of this study are included within the article (and any supplementary files).

ORCID iDs

Rishabh Kumar https://orcid.org/0000-0002-4160-4607
Rinku Prajapat https://orcid.org/0000-0003-3555-3126
Moumita Maiti https://orcid.org/0000-0001-9460-4347

References

[1] Hagino k and Takigawa N 2012 *Prog. Theor. Phys.* **128** 1061
[2] Canto L F, Gomes P R S, Donangelo R, Lubian J and Hussein M S 2015 *Phys. Rep.* **596** 1
[3] Jha V, Parkar V V and Kailas S 2020 *Phys. Rep.* **845** 1
[4] Zhang N T *et al* 2014 *Phys. Rev.* C **90** 024621
[5] Kaushik M *et al* 2021 *Phys. Rev.* C **104** 024615
[6] Shrivastava A *et al* 2009 *Phys. Rev. Lett.* **103** 232702
[7] Kumar D, Maiti M and Lahiri S 2017 *Phys. Rev.* C **96** 014617

[8] Kumar D, Maiti M and Lahiri S 2016 *Phys. Rev.* C **94** 044603
[9] Gasques L R, Hinde D J, Dasgupta M, Mukherjee A and Thomas R G 2009 *Phys. Rev.* C **79** 034605
[10] Shuaib M *et al* 2016 *Phys. Rev.* C **94** 014613
[11] Prajapat R and Maiti M 2020 *Phys. Rev.* C **101** 024608
[12] Chauhan A and Maiti M 2019 *Phys. Rev.* C **99** 034608
[13] Trautmann W, Hansen O, Tricoire H, Hering W, Ritzka R and Trombik W 1984 *Phys. Rev. Lett.* **53** 1630
[14] Guo C L *et al* 2015 *Phys. Rev.* C **92** 014615
[15] Dasgupta M *et al* 2004 *Phys. Rev.* C **70** 024606
[16] Gomes P R S *et al* 2005 *Phys. Rev.* C **71** 034608
[17] Shaikh M M, Roy S, Rajbanshi S, Pradhan M K, Mukherjee A, Basu P, Pal S, Nanal V, Pillay R G and Shrivastava A 2014 *Phys. Rev.* C **90** 024615
[18] Kumawat H *et al* 2012 *Phys. Rev.* C **86** 024607
[19] Hu S P *et al* 2015 *Phys. Rev.* C **91** 044619
[20] Parkar V V *et al* 2018 *Phys. Rev.* C **97** 014607
[21] Rath P K *et al* 2009 *Phys. Rev.* C **79** 051601(R)
[22] Rath P K *et al* 2012 *Nucl. Phys.* A **874** 14
[23] Pradhan M K *et al* 2011 *Phys. Rev.* C **83** 064606
[24] Palshetkar C S *et al* 2014 *Phys. Rev.* C **89** 024607
[25] Wu Y W, Liu Z H, Lin C J, Zhang H Q, Ruan M, Yang F, Li Z C, Trotta M and Hagino K 2003 *Phys. Rev.* C **68** 044605
[26] Kumar R, Maiti M, Sarkar G, Sagwal M, Kaur P, Nag T N and Sodaye S 2021 *Eur. Phys. J.* A **57** 209
[27] Kumar R, Maiti M, Nag T N and Sodaye S 2021 *Phys. Rev.* C **104** 064606
[28] Prajapat R and Maiti M 2021 *Phys. Rev.* C **103** 034620
[29] Kumar D and Maiti M 2017 *Phys. Rev.* C **96** 044624
[30] Prajapat R and Maiti M 2020 *Phys. Rev.* C **101** 064620
[31] Ziegler J F, Ziegler M D and Biersack J P 2010 *Nucl. Instrum. Methods Phys. Res.* B **268** 1818
[32] Maiti M and Lahiri S 2010 *Phys. Rev.* C **81** 024603
[33] Prajapat R, Maiti M and Kumar D 2021 *Phys. Rev.* C **103** 014608
[34] National Nuclear Data Center, Brookhaven National Laboratory, (http://nndc.bnl.gov/nudat3/)
[35] Baglin C M 2016 *Nucl. Data Sheets* **134** 149
[36] Wilken B and Fritz T A 1976 *Nucl. Instrum. Methods* **138** 331
[37] Gavron A 1980 *Phys. Rev.* C **21** 230
[38] Herman M, Capote R, Carlson B V, Oblozinsky P, Sin M, Trkov A, Wienke H and Zerkin V 2007 *Nucl. Data Sheets* **108** 2655
[39] Perey C M and Perey F G 1976 *At. Data Nucl. Data Tables* **17** 1
[40] Bass R 1977 *Phys. Rev. Lett.* **39** 265
[41] Hill D and Wheeler J 1953 *Phys. Rev.* **89** 1102
[42] Dasso C H and Landowne S 1987 *Comput. Phys. Commun.* **46** 187
[43] Koning A J and Delaroche J P 2003 *Nucl. Phys.* A **713** 231
[44] An H and Cai C 2006 *Phys. Rev.* C **73** 054605
[45] Becchetti F D Jr and Greenless G W 1969 *Phys. Rev.* **182** 1190
[46] Avrigeanu V, Hodgson P E and Avrigeanu M 1994 *Phys. Rev.* C **49** 2136
[47] Cavinato M, Fabrici E, Gadioli E, Gadioli Erba E, Vergani P, Crippa M, Colombo G, Redaelli I and Ripamonti M 1995 *Phys. Rev.* C **52** 2577
[48] Chattopadhyay D *et al* 2016 *Phys. Rev.* C **94** 061602(R)
[49] Zhang G L *et al* 2018 *Phys. Rev.* C **97** 014611
[50] Souza F A *et al* 2009 *Nucl. Phys.* A **821** 36
[51] Castaneda C M, Smith H A Jr, Singh P P and Karwowski H 1980 *Phys. Rev.* C **21** 179
[52] Shrivastava A, Navin A, Keeley N, Mahata K, Ramachandran K, Nanal V, Parkar V V, Chatterjee A and Kailas S 2006 *Phys. Lett.* B **633** 463
[53] Udagawa T and Tamura T 1980 *Phys. Rev. Lett.* **45** 1311
[54] Wilczynski J *et al* 1980 *Phys. Rev. Lett.* **45** 606
[55] Gomes P R S *et al* 2006 *Phys. Rev.* C **73** 064606
[56] Thompson I J 1988 *Comput. Phys. Rep.* **7** 167
[57] Figueira J M *et al* 2010 *Phys. Rev.* C **81** 024613

[58] Kovar D G, Stein N and Bockelman C K 1974 *Nucl. Phys.* A **231** 266
[59] Cook J 1982 *Nucl. Phys.* A **388** 153
[60] Brown B A and Rae W D M 2014 *Nucl. Data Sheets* **120** 115
[61] Cohen S and Kurath D 1965 *Nucl. Phys.* **73** 1
[62] Tsang M B, Lee J and Lynch W G 2005 *Phys. Rev. Lett.* **95** 222501
[63] Möller P, Sierk A J, Ichikawa T and Sagawa H 2012 *At. Data Nucl. Data Tables* **109-110** 1
[64] Walker P and Podolyák Z 2020 *Phys. Scr.* **95** 044004
[65] Mukherjee S, Singh N L, Kumar G K and Chaturvedi L 2005 *Phys. Rev.* C **72** 014609